SPAK-p38 MAPK Signal Pathway Modulates Claudin-18 and Barrier Function of Alveolar Epithelium after Hyperoxic Exposure

Chih-Hao Shen
Tri-Service General Hospital https://orcid.org/0000-0002-3910-1269
Jr-Yu Lin
National Defense Medical Center
Cheng-Yo Lu
National Defense Medical Center
Sung-Sen Yang
Tri-Service General Hospital
Chung-Kan Peng
Tri-Service General Hospital
Kun-Lun Huang (kun@mail.ndmctsgh.edu.tw)
Tri-Service General Hospital

Research article

Keywords: STE20/SPS1-related proline/alanine-rich kinase, hyperoxia, alveolar epithelium, claudin-18, p38 MAPK

Posted Date: December 10th, 2020

DOI: https://doi.org/10.21203/rs.3.rs-122497/v1

Version of Record: A version of this preprint was published on February 15th, 2021. See the published version at https://doi.org/10.1186/s12890-021-01408-7.

Abstract

Background: Hyperoxia downregulates the tight junction (TJ) proteins of the alveolar epithelium and leads to barrier dysfunction. Previous study has showed that STE20/SPS1-related proline/alanine-rich kinase (SPAK) interferes with the intestinal barrier function in mice. The aim of the present study is to explore the association between SPAK and barrier function in the alveolar epithelium after hyperoxic exposure.

Methods: Hyperoxic acute lung injury (HALI) was induced by exposing mice to >99% oxygen for 64 hours. The mice were randomly allotted into four groups comprising two control groups and two hyperoxic groups with and without SPAK knockout. Mouse alveolar MLE-12 cells were cultured in control and hyperoxic conditions with or without SPAK knockdown. Transepithelial electric resistance and transwell monolayer permeability were measured for each group. In-cell western assay was used to screen the possible mechanism of p-SPAK being induced by hyperoxia.

Results: Compared with the control group, SPAK knockout mice had a lower protein level in the bronchoalveolar lavage fluid in HALI, which was correlated with a lower extent of TJ disruption according to transmission electron microscopy. Hyperoxia down-regulated claudin-18 in the alveolar epithelium, which was alleviated in SPAK knockout mice. In MLE-12 cells, hyperoxia up-regulated phosphorylated-SPAK by reactive oxygen species (ROS), which was inhibited by indomethacin. Compared with the control group, SPAK knockdown MLE-12 cells had higher transepithelial electrical resistance and lower transwell monolayer permeability after hyperoxic exposure. The expression of claudin-18 was suppressed by hyperoxia, and down-regulation of SPAK restored the expression of claudin-18. The process of SPAK suppressing the expression of claudin-18 and impairing the barrier function was mediated by p38 mitogen-activated *protein kinase* (MAPK).

Conclusions: Hyperoxia up-regulates the SPAK-p38 MAPK signal pathway by ROS, which disrupts the TJ of the alveolar epithelium by suppressing the expression of claudin-18. Down-regulation of SPAK attenuates this process and protects the alveolar epithelium against the barrier dysfunction induced by hyperoxia.

Background

Supplemental oxygen is used to counteract tissue hypoxemia, but breathing a high concentration of oxygen for a prolonged period may cause fatally hyperoxic acute lung injury (HALI) in both adults and premature infants [1–3]. HALI presents with histopathological changes that include increased microvascular permeability, the influx of protein-rich fluid, and the formation of lung edema, which are similar to the changes seen in the acute respiratory distress syndrome. In HALI, reactive oxygen species (ROS) are generated due to prolonged hyperoxia and destroy alveolar epithelial cells through both necrosis and apoptosis [3, 4]. Hyperoxia also results in the accumulation of inflammatory mediators within the lungs. This process involves protein kinases such as serine-threonine kinase Akt, mitogen-

activated protein kinases (MAPK), protein kinase C, and transcription factors such as NF-E2-related transcription factor 2 and nuclear factor-κB [5, 6].

In the alveolar epithelium, transmembrane and peripheral proteins compose the tight junction (TJ) that attach cells tightly to their neighbors and form a barrier. The change of TJ modulates the paracellular space and plays an important role in maintaining the hydration, ionic, and solute balance of alveoli [7, 8]. Three transmembrane protein families are found in the TJ: occludins, claudins, and junctional adhesion molecules [9, 10]. TJ proteins that are frequently expressed in the lungs include claudin-1, claudin-3, claudin-4, claudin-5, claudin-7, claudin-18, occludin, ZO-1, and ZO-2 [11–13]. Previous studies have shown that hyperoxia downregulates the expression of TJ proteins in the alveolar epithelium in HALI, which leads to barrier dysfunction [14–16].

STE20/SPS1-related proline/alanine-rich kinase (SPAK) is a member of the SPS1 subfamily of the mammalian STE20-related protein kinase family and is expressed ubiquitously throughout the body [17]. In the alveolar epithelium, SPAK is a downstream substrate of WNK4 kinase and an upstream regulator of Na-K-Cl cotransporter 1(NKCC1) [18]. The phosphorylation of SPAK during osmotic stress regulates the activity of NKCC1 and maintains alveolar fluid homeostasis [19]. The role of the WNK4-SPAK-NKCC1 pathway involved in lung injury have been investigated previously. The mice with SPAK knockout exhibited longer survival than wild-type controls in HALI. In this study, SPAK may interfere with the course of lung injury by modulating alveolar fluid clearance via NKCC1 [20].

In addition to NKCC1, SPAK modulates other downstream effectors that are involved in the formation of epithelial barrier. In a model of intestinal inflammation, the production of inflammatory cytokines and aggravated bacterial translocation were facilitated in SPAK transgenic mice [21]. Another study showed that mice with SPAK deficiency had less proinflammatory cytokine production and luminal bacteria translocation [22]. In these two studies, changes in transepithelial resistance were observed [21, 22]. However, no study has explored the association between SPAK and the barrier function of the alveolar epithelium. The present study explores the role of SPAK in hyperoxia-induced alveolar barrier dysfunction both in vitro and in vivo.

Methods

Transgenic SPAK knockout mice

The mouse mutants for SPAK were provided by Dr Sung-Sen Yang (National Defense Medical Center, Taipei, Taiwan). SPAK+/– littermates were generated as described previously [23, 24]. SPAK+/– littermates were intercrossed to generate SPAK–/– (SPKA-KO) and wild-type (WT) mice. Approval for the project protocol was obtained from the Institutional Animal Care and Use Committee of the National Defense Medical Center. The mice were bred and maintained in pathogen-free animal facilities at the Laboratory Animal Center of the National Defense Medical Center (Taipei, Taiwan).

Animal model of hyperoxic acute lung injury

The study was performed with 10 to 12-week-old male mice. The mice were randomly allotted into four groups comprising two control groups and two hyperoxic groups with and without SPAK knockout (n = 6 per group; totally 24 mice were used). We achieved random allocation by tossing a coin. In the control group, mice were kept in identical chambers and exposed to room air only (n = 6 per cage). In the hyperoxic group, mice were exposed to >99% oxygen in an airtight chamber with a ventilation flow of 5 L/min for 64 hours (n = 6 per cage). The CO_2 concentration was kept at <0.1%, and the temperature was controlled between 25 and 26°C. In each cage, all mice were provided access to food and water ad libitum to minimise potential confounders such as the order of measurements and animal location.

At the end of the animal experiment, the mice were anaesthetized through intraperitoneal injection of Zoletil (Virbac, Carros, France; 35 mg/kg body weight) and Rompun (Bayer, Leverkusen, Germany; 10 mg/kg body weight). We performed a tracheostomy and a median sternotomy under general anesthesia. Then, the mice were euthanized by cardiac puncture before regaining consciousness. After euthanasia, bronchoalveolar lavage fluid (BALF) was obtained by lavaging the left lung twice with 0.5 mL of saline from the tracheostomy. The blood samples and right lung tissues were collected for further evaluation.

Histopathology

The numbers of polymorphonuclear neutrophils and lung injury score in the lung tissue were analyzed. In brief, the lung tissues were fixed, sectioned, and stained with eosin and hematoxylin. Morphological examinations were performed using light microscopy. A minimum of 10 randomly selected fields were examined for neutrophil infiltration in the airspace or vessel wall. The thickening of the alveolar wall was also observed. The lung damage was scored as follows using a four-point scale: none (0), mild (1), moderate (2), or severe (3). The scoring was performed by two pathologists who were blinded to the experimental conditions. The two resulting scores were summed to represent the lung injury score.

Bronchoalveolar lavage fluid protein

The BALF was centrifuged at 200g for 10 minutes to remove all cells and cellular debris. The protein concentrations were determined using a Pierce™ BCA protein assay kit (Thermo Fisher Scientific).

Transmission electron microscopy

Ultrastructural characterization of the cytological alterations was performed by a following a procedure that is detailed in previous publication. Briefly, lung tissue blocks (maximal 1 mm^3) were immediately dissected after euthanasia, kept overnight at 4°C in fixative (4% paraformaldehyde and 2.5% glutaraldehyde in 1xPBS; pH 7.4), and postfixed in 1% OsO_4 in the same buffer. After dehydration in graded ethanol the blocks were finally embedded in Spurr's resin (Spurr Low Viscosity Embedding Kit; EMS ®). Semithin sections (0.5µm thick) were cut with a glass knife on a Leica EM UC7 ultramicrotome and stained with toluidine blue. For TEM, ultrathin sections were cut on a Leica® Ultracut UC7 Ultramicrotome with a diamond knife. The sections were stained with uranyl acetate and lead citrate and examined with a FEI Tecnai G2 F20 S-TWIN Electron Microscope at 120 kV.

MLE-12 cells and exposure to hyperoxia

MLE-12 cells, the type II mouse-lung epithelial cell, were purchased from ATCC (Manassas, VA). Cells were cultured in a 50:50 mixed medium of DMEM and Ham's F-12 supplemented with 4% FBS, insulin (5 μg/mL), transferrin (10 μg/mL), sodium selenite (30 nM), hydrocortisone (10 nM), β-estradiol (10 nM), HEPES (10 nM), and L-glutamine (2 mM). In transgenic studies, MLE-12 cells were cultured on 6-well plates. At 60–75% confluence, transient transfection was carried out using SPAK siRNA (50 nM) (Dharmacon RNA Technologies) as the SPAK-knockdown (SPAK-KD) or siCONTROL Non-Targeting siRNA (50 nM) as the negative control. In the hyperoxic group, cells were placed in an incubator filled with 95% O_2 and 5% CO_2 at 37°C for 48 hours. In the control group, cells were kept in 21% O_2 and 5% CO_2 at 37°C for 48 hours.

Transepithelial electric resistance measurements

Electric cell-substrate impedance sensing (ECIS) measurements were performed using 8W1E+ electrode arrays on an ECIS Zθ instrument (Applied Biophysics, Troy, NY). The measurements were performed as described previously [25, 26]. A baseline was established using culture medium (400 μL·well^{-1}). The resistance was recorded in units of Ω at a frequency of 500 Hz. At 48 hours after transfection, the cells were sub-cultured on an ECIS array. Exposure to hyperoxia or normoxia began when the electrode was covered with a monolayer of cells. The ECIS allows for a sensitive determination of the amount of current passing between cells and the resistance of the barrier (*Rb*) (in units of Ω cm^2). *Rb* is a robust reporter of barrier function [27].

Transwell monolayer permeability assay

To measure the paracellular permeability, MLE-12 cells were grown as a monolayer in 6.5-mm-diameter transwell filter inserts with a pore size of 3.0 μm (Corning Life Sciences, Lowell, MA). After 48 hours of exposure to hyperoxia, the medium of the upper chamber was replaced with medium containing albumin-fluorescein isothiocyanate (4 kDa, 2 mg/ml). Four hours later, 100-μL samples from the lower chambers were collected and analyzed for fluorescein isothiocyanate intensity using a fluorometric plate reader with an excitation of 494 nm and emission at 520 nm.

Immunofluorescence staining

Immunofluorescence staining was performed using a published procedure [28]. We treated lung sections with primary rabbit polyclonal antibody, claudin-18 (diluted 1:200, Proteintech, IL, USA), and phosphorylated-SPAK (p-SPAK) (diluted 1:100, OriGene, MD, USA) for immunofluorescent labeling. The secondary antibody was goat anti-mouse IgG-FITC (diluted 1:200, Santa Cruz Biotechnology, USA) and Rhodamine (TRITC) AffiniPure Goat Anti-Rabbit IgG (diluted 1:200, Jackson ImmunoResearch Inc. PA, USA). The slides were mounted with VECTASHIELD Antifade Mounting Medium (Vector Laboratories, Inc. CA, USA) and DAPI. Images were obtained using a DeltaVision system (Applied Precision) comprising a

wide-field inverted microscope (model IX-71; Olympus) with ×60/1.42 Plan Apo N or ×100/1.40 Super-Plan APO objectives.

In-cell western assay

An in-cell western assay was performed using an Odyssey Infrared Imaging System (LICOR Biosciences, NE, USA). The cells were cultured at a density of 1.2×10^4 cells/well in 96-well culture plates and incubated overnight in complete culture medium. At 70% confluence, the cells were pre-treated with ROS inhibitors for 30 minutes and then exposed to hyperoxia for 24 hours. Cells were fixed with refrigerated 75% EtOH and stained with phosphorylated SPAK (Ser311) (diluted 1:200, OriGene, Rockville, MD) and beta-actin (diluted 1:200, Sigma Chemical Company, MO, USA) at 4°C overnight. Anti-rabbit IRDye® 680RD-labeled (1:5000) and anti-mouse IRDye® 800-labeled CW (1:5000) antibodies (LICOR Biosciences, NE, USA) were used as secondary antibodies at room temperature for 1 hour and were detected by the 700 and 800-nm channels, respectively.

Western blot analysis

Western blot analyses were performed based on a standard protocol with the relevant antibodies: claudin-18 (diluted 1:200, Thermo Fisher Scientific Inc, IL, USA), p-SPAK (diluted 1:1000, OriGene, MD, USA), phosphorylated-p38 (p-p38) (diluted 1:1000, Cell Signaling Technology, USA), total-p38 (T-p38) (diluted 1:1000, Cell Signaling Technology, USA), beta-actin (diluted 1:1000, Sigma Chemical Company, MO, USA) and GAPDH (diluted 1:1000, Thermo Fisher Scientific Inc, IL, USA).

Real-time PCR

Total RNA was isolated using an RNA-spin total RNA extraction kit (Intron Biotechnology, Korea) according to the manufacturer's instructions. The synthesis of cDNA was performed with 2 μg of RNA using a High-Capacity cDNA Archive Kit (Applied Biosystems, CA, USA). Quantitative real-time PCR was performed for claudin-18 (Mm00517322_m1) and GAPDH (Mm99999915_g1) using TaqMan assays (Applied Biosystems, CA, USA). Each sample was analyzed in triplicate on a 96-well plate, which was centrifuged briefly and placed in a QuantStudio™ 5 Real-Time PCR System (Thermo Fisher Scientific, MA, USA). The analysis was performed using the following program: 2 min at 50◦C, 10 min at 95◦C, and 40 cycles of 15 s at 95◦C and 1 min at 60◦C. The relative gene expression was calculated using the $2^{-\Delta\Delta CT}$ method.

Statistical analysis

We performed statistical analyses using GraphPad Prism v. 5.00 for Windows. All results are expressed as the mean ± standard deviation of the mean. There was no data point that was not included in the analysis. We used one-way analysis of covariance (ANOVA) to compare the differences between the study groups, and then Bonferroni's correction was employed for post-hoc comparisons. A p-value < 0.05 was considered significant.

Results

SPAK knockout mice preserves barrier integrity in mice with hyperoxic acute lung injury

Histological evaluation of the lung tissues indicated a higher lung injury score after hyperoxic exposure for 64 hours. Knockout SPAK significantly mitigated the increases in lung injury score (Fig. 1A, 1B). The protein concentration of BALF was measured as an indicator of dysfunction in the alveolar capillary barrier. After hyperoxia, the protein concentration increased significantly. SPAK-KO mice had significantly lower protein concentrations than WT mice (Fig. 1C). Transmission electron microscopy was used to evaluate the morphology of TJ in the alveolar epithelial cells of mice after hyperoxic exposure. In lung tissue from WT mice, the apical side indicated a loss of TJ and the presence of paracellular gaps between alveolar epithelial cells. Lung tissue from SPAK-KO mice showed a lesser extent of TJ disruption (Fig. 1D). The protein concentration of BALF was correlated with the extent of TJ disruption.

Phosphorylation of SPAK mediates the decline in claudin-18 expression of the alveolar epithelium in mice with hyperoxic acute lung injury

The p-SPAK and claudin-18 of alveolar epithelium were observed by lung tissue immunofluorescence double staining. Markedly increased p-SPAK in the alveolar epithelium of WT mice exposed to hyperoxia for 64 hours was noted, and the increase was significantly less pronounced in the SPAK-KO mice. The expression of claudin-18 in the alveolar epithelium was significantly lower in the hyperoxic group than the normoxic group in WT mice. In SPAK-KO mice, the expression of claudin-18 was restored in the hyperoxic group (Fig. 2A). The effects of hyperoxia in activating p-SPAK and SPAK-KO in maintaining claudin-18 expression after hyperoxia were validated by western blot analysis for the lung tissues (Fig. 2B, 2C).

Hyperoxia Up-regulates Phosphorylated-spak By Ros In Mle-12 Cells

MLE-12 cells were treated with hyperoxia to assess the change of p-SPAK in the alveolar epithelium. The p-SPAK was significantly activated after exposure to hyperoxia for 24 hours (Fig. 3A). To assess the effects of ROS in activating p-SPAK, MLE-12 cells were pretreated with n-acetylcysteine (NAC) and then treated with hyperoxia. The p-SPAK was activated by hyperoxia, and pretreatment with a NAC concentration of 5 mM suppressed this activation (Fig. 3B). To screen the possible mechanism of p-SPAK being induced by ROS, an in-cell western assay was used for MLE-12 cells exposed to 24 hours of hyperoxia. ROS-generating enzyme inhibitors were applied as pretreatment before hyperoxia, including apocynin, indomethacin, ketoconazole, NADG, rotenone, allopurinol, and L-NAME. The activation of p-SPAK was not suppressed by low concentrations of ROS-generating enzyme inhibitors, but it was significantly suppressed by a high concentration of indomethacin (Fig. 3C). Western blot analysis validated the effect of indomethacin in hyperoxia-induced p-SPAK activation (Fig. 3D).

SPAK mediates the decline in claudin-18 expression and barrier function of MLE-12 cells after hyperoxic exposure

We measured the expression of claudin-18 in MLE-12 cells and found that hyperoxia suppressed the expression in a time-dependent manner. A significant decrease was noted after 48 hours of exposure (Fig. 4A). We performed immunoblotting and quantitative real-time PCR to demonstrate the effect of SPAK on the expression of claudin-18 in MLE-12 cells exposed to hyperoxia for 48 hours. The claudin-18 expression was significantly decreased in the control group in comparison to the SPAK-KD group (Figs. 4B, 4C). We measured the transepithelial electrical resistance of the monolayer of MLE-12 cells by ECIS to assess the effect of SPAK on the barrier integrity of the alveolar epithelium. A lower resistance (at a frequency of 500 Hz in ECIS measurements) was observed in the control group. The decrease of resistance caused by hyperoxic exposure was restored in the SPAK-KD group (Fig. 4D). The *Rb* decreased significantly after hyperoxic exposure in the control group, but not in the SPAK-KD group (Fig. 4E). In addition, hyperoxic exposure resulted in an increased paracellular permeability, which was alleviated by knocking down SPAK (Fig. 4F). These findings suggest that down-regulating SPAK attenuates the hyperoxia-induced barrier dysfunction in the alveolar epithelium.

SPAK modulates hyperoxia-induced barrier dysfunction and suppression of claudin-18 via p38 MAPK in MLE-12 cells

A previous study showed that SPAK acts as a mediator of stress-activated signals that activates p38 MAPK [29]. We performed immunoblotting of T-p38 and p-p38 expressions in MLE-12 cells exposed to hyperoxia for 24 and 48 hours (Figs. 5A, 5B). The expression of p-p38 was activated by hyperoxia in the control group. In the SPAK-KD group, the expression decreased significantly. The role of p38 MAPK in modulating the expression of claudin-18 was assessed by pretreating MLE-12 cells with 2 μM of p38 MAPK inhibitor (BIRB-796), followed by hyperoxia for 48 hours. Hyperoxia resulted in lower claudin-18 expression, which was restored by BIRB0796 (Figs. 5C, 5D). ECIS showed that pretreatment with p38 MAPK inhibitor restored the decrease of resistance in MLE-12 cells after hyperoxic exposure (Fig. 5E). The *Rb* decreased significantly in the control group after hyperoxic exposure, but not in the p38 MAPK inhibitor group (Fig. 5F). These findings indicate that SPAK modulates hyperoxia-induced barrier dysfunction and the suppression of claudin-18 via p38 MAPK in the alveolar epithelium.

Discussion

This study investigated the role of SPAK in the hyperoxia-induced barrier dysfunction of the alveolar epithelium. Hyperoxia activates p-SPAK by ROS, which disrupts the TJ of the alveolar epithelium by suppressing the expression of claudin-18. Down-regulation of SPAK protects the alveolar epithelium against the barrier dysfunction induced by hyperoxia. In the present study, the cellular model represents the condition of SPAK-KD acting on the alveolar epithelium. Our findings highlight a direct effect of the SPAK-p38 MAPK signal pathway on epithelial claudin-18 expression and barrier function.

We found that both hyperoxia up-regulated the levels of p-SPAK, and the antioxidant NAC suppressed these responses in the alveolar epithelium. This suggests that hyperoxia activated p-SPAK of the alveolar epithelium by ROS. ROS is a family of active molecules containing free radicals that are involved in the injury of various cellular constituents, such as lipids, proteins, and DNA [30]. For epithelial cells, ROS disrupts the TJ directly by protein modifications such as thiol oxidation, phosphorylation, nitration, and carbonylation. Multiple inflammatory pathways may also be stimulated to impair the TJ and barrier function [13, 31, 32]. The known ROS-producing enzymes in mammalian cells are NADPH oxidases, xanthine oxidase, lipoxygenases, and cytochrome P450 [33]. ROS activates cyclooxygenase, and the activation of cyclooxygenase/prostaglandin synthase pathways may induce further ROS production through effects on different ROS-generating enzymes [34]. We found that p-SPAK activation induced by ROS was significantly inhibited by indomethacin, a cyclooxygenase inhibitor, suggesting that cyclooxygenase may play an essential role in activating p-SPAK in HALI.

We found that the up-regulation of p-SPAK impaired the alveolar barrier function. The expression of claudin-18 was correlated with the extent of TJ disruption in HALI and was restored by down-regulating p-SPAK. Claudin-18 is the claudin that is overwhelmingly expressed by alveolar epithelial cells [35]. In a bleomycin-induced experimental model of lung injury, the expression of claudin-18 and the integrity of the epithelial TJ were disturbed in the fibrotic lesions [36]. Claudin-18 may play an important role in the regulation of ion selectivity to mediate barrier function. A previous study has shown that claudin-18 knockout mice exhibit greater solute permeability than WT control mice. In monolayers formed by claudin-18-deficient alveolar epithelial cells, enlarged paracellular gaps were correlated with changes in the actin cytoskeleton [37]. Therefore, claudin-18 may be a crucial target modulated by SPAK in the alveolar epithelium after hyperoxic exposure.

In a mouse model of intestinal inflammation, SPAK altered the permeability of epithelial cells by regulating the expression of TJ proteins. SPAK-KO mice showed increased barrier function of the intestinal epithelium induced by dextran sulfate sodium. The changes of barrier function were associated with increased expressions of occludin, E-cadherin, β-catenin, and claudin-5, but there were no noticeable changes in the expressions of claudin-1, claudin-4, ZO-1, and ZO-2 [22]. Claudin-18 was not affected in this study, and we suppose that this may have been caused by the differences in the injury model and injured tissue. Further studies are warranted to identify the associations between SPAK and changes in other TJ proteins induced by hyperoxia.

We found that SPAK modulated p38 MAPK and hyperoxia-induced barrier dysfunction. Many factors contribute to the biological interactions with SPAK. SPAK functions as an upstream kinase of NKCC1, but previous studies have not shown associations between NKCC1 and epithelial barrier function. SPAK has several binding partners and effectors, such as apoptosis-associated tyrosine kinase, protein kinase C isotypes, glycoprotein CD46, heat shock protein, otoferlin, gelsolin, calcium binding protein, p21-activated protein kinase, and MAPKs [38]. Among these kinases, activation of p38 MAPK was found in mice with LPS-induced acute lung injury, and inhibition of p38 MAPK activity attenuated pulmonary edema formation and hyperpermeability [39]. A previous study has shown that ROS contributes to the activation

of p38 MAPK, which was associated with microtubule destabilization and the formation of paracellular gaps in the vascular endothelium in mouse lungs [34]. In our study, the expression of claudin-18 was also modulated by p38 MAPK in the alveolar epithelium when exposed to hyperoxia, which points out the multiple roles of p38 MPAK in barrier dysfunction induced by oxidative stress.

The main limitation of this study is the complex pathogenic condition of HALI. In the present study, we found that SPAK activated p-p38 in MLE-12 cells exposed to hyperoxia. However, hyperoxia triggers diverse effects that involve not only the alveolar epithelium and the pulmonary vascular endothelium, but also the inflammatory cells such as macrophages and neutrophils [7, 8]. Although the cellular model in the present study demonstrates a direct benefit of SPAK-KD on the alveolar epithelium exposed to hyperoxia, the effects of SPAK on other cells remain uncertain. Further studies are warranted to identify the roles of SPAK in the crosstalk between epithelium, endothelium, and inflammatory cells in HALI.

Conclusions

We have presented the first research exploring the association between SPAK and barrier function of alveolar epithelium when exposed to hyperoxia both in vivo and in vitro. Hyperoxia up-regulates the SPAK-p38 MAPK signal pathway by ROS, which disrupts the TJ of the alveolar epithelium by suppressing the expression of claudin-18. Down-regulation of SPAK attenuates this process. Selective inhibition of SPAK phosphorylation in the alveolar epithelium may be a potential strategy to alleviate hyperoxia-indued barrier dysfunction in HALI.

Abbreviations

TJ
tight junction
SPAK
STE20/SPS1-related proline/alanine-rich kinase
HALI
hyperoxic acute lung injury
ROS
reactive oxygen species
MAPK
mitogen-activated protein kinase
NKCC1
Na-K-Cl cotransporter 1
WT
wild-type
LPS
lipopolysaccharide
SPAK-KO

SPAK knockout

BALF

bronchoalveolar lavage fluid

ECIS

electric cell-substrate impedance sensing

p-SPAK

phosphorylated-SPAK

p-p38

phosphorylated-p38

T-p38

total-p38

NAC

n-acetylcysteine

SPAK-KD

SPAK-knockdown

Declarations

Ethics approval and consent to participate

The experimental animals were handled in accordance with a protocol approved by the National Science Council and Animal Review Committee at the National Defense Medical Center.

Consent for publication

Not applicable.

Availability of data and materials

The data generated during this study are included in this published article and its supplementary information files.

Competing interests

The authors declare that they have no competing interests related to this publication.

Funding

This work was supported by grants from Ministry of Science and Technology, Taiwan (MOST 105-2314-B-016-003), Tri-Service General Hospital (Award numbers: TSGH-C106-069, TSGH-E-109228), and Ministry of National Defense-Medical Affairs Bureau (Award numbers: MAB-106-015, MAB-109-019). No funding provider had any influence on the design of the study or the collection, analysis, and interpretation of data or the content of this paper.

Authors' contributions

CHS: drafting of manuscript; CHS and KLH: study conception and design, interpretation of data; CHS, JYL, and CYL: acquisition of data, analysis of data; SSY, CKP, and KLH: manuscript review. All authors read and approved the final manuscript.

Acknowledgements

We would like to acknowledge Instrument Center of National Defense Medical Centre for the technical supports.

References

1. Bhandari V. Hyperoxia-derived lung damage in preterm infants. Semin Fetal Neonatal Med. 2010;15(4):223–9.
2. Altemeier WA, Sinclair SE. Hyperoxia in the intensive care unit: why more is not always better. Curr Opin Crit Care. 2007;13(1):73–8.
3. Kallet RH, Matthay MA. Hyperoxic acute lung injury. Respir Care. 2013;58(1):123–41.
4. Pagano A, Barazzone-Argiroffo C. Alveolar cell death in hyperoxia-induced lung injury. Ann N Y Acad Sci. 2003;1010:405–16.
5. Gore A, Muralidhar M, Espey MG, Degenhardt K, Mantell LL. Hyperoxia sensing: from molecular mechanisms to significance in disease. J Immunotoxicol. 2010;7(4):239–54.
6. Porzionato A, Sfriso MM, Mazzatenta A, Macchi V, De Caro R, Di Giulio C. Effects of hyperoxic exposure on signal transduction pathways in the lung. Respir Physiol Neurobiol. 2015;209:106–14.
7. Schneeberger EE, Lynch RD. Structure, function, and regulation of cellular tight junctions. Am J Physiol. 1992;262(6 Pt 1):L647–61.
8. Herrero R, Sanchez G, Lorente JA. New insights into the mechanisms of pulmonary edema in acute lung injury. Ann Transl Med. 2018;6(2):32–2.
9. Blasig IE, Haseloff RF. Tight junctions and tissue barriers. Antioxid Redox Signal. 2011;15(5):1163–6.
10. Fanning AS, Anderson JM. Zonula Occludens-1 and – 2 Are Cytosolic Scaffolds That Regulate the Assembly of Cellular Junctions. Ann N Y Acad Sci. 2009;1165(1):113–20.
11. Overgaard CE, Mitchell LA, Koval M. Roles for claudins in alveolar epithelial barrier function. Ann N Y Acad Sci. 2012;1257(1):167–74.
12. Frank JA. Claudins and alveolar epithelial barrier function in the lung. Ann N Y Acad Sci. 2012;1257:175–83.
13. Blasig IE, Bellmann C, Cording J, Del Vecchio G, Zwanziger D, Huber O, Haseloff RF. Occludin protein family: oxidative stress and reducing conditions. Antioxid Redox Signal. 2011;15(5):1195–219.
14. Xu S, Xue X, You K, Fu J. Caveolin-1 regulates the expression of tight junction proteins during hyperoxia-induced pulmonary epithelial barrier breakdown. Respiratory research. 2016;17(1):50–0.

15. Vyas-Read S, Vance RJ, Wang W, Colvocoresses-Dodds J, Brown LA, Koval M. Hyperoxia induces paracellular leak and alters claudin expression by neonatal alveolar epithelial cells. Pediatr Pulmonol. 2018;53(1):17–27.
16. Al-Shmgani HS, Moate RM, Macnaughton PD, Sneyd JR, Moody AJ. Effects of hyperoxia on the permeability of 16HBE14o- cell monolayers–the protective role of antioxidant vitamins E and C. FEBS J. 2013;280(18):4512–21.
17. Gagnon KB, Delpire E. Molecular Physiology of SPAK and OSR1: Two Ste20-Related Protein Kinases Regulating Ion Transport. Physiological reviews. 2012;92(4):1577–617.
18. Gagnon KB, England R, Delpire E. A single binding motif is required for SPAK activation of the Na-K-2Cl cotransporter. Cellular physiology biochemistry: international journal of experimental cellular physiology biochemistry pharmacology. 2007;20(1–4):131–42.
19. Richardson C, Alessi DR. The regulation of salt transport and blood pressure by the WNK-SPAK/OSR1 signalling pathway. Journal of cell science. 2008;121(Pt 20):3293–304.
20. Lin HJ, Wu CP, Peng CK, Lin SH, Uchida S, Yang SS, Huang KL. With-No-Lysine Kinase 4 Mediates Alveolar Fluid Regulation in Hyperoxia-Induced Lung Injury. Critical care medicine. 2015;43(10):e412–9.
21. Yan Y, Laroui H, Ingersoll SA, Ayyadurai S, Charania M, Yang S, Dalmasso G, Obertone TS, Nguyen H, Sitaraman SV, et al: **Over-expression of Ste20-related proline/alanine rich kinase (SPAK) exacerbates experimental colitis in mice**. *Journal of immunology (Baltimore, Md: 1950)* 2011, **187**(3):1496–1505.
22. Zhang Y, Viennois E, Xiao B, Baker MT, Yang S, Okoro I, Yan Y. Knockout of Ste20-Like Proline/Alanine-Rich Kinase (SPAK) Attenuates Intestinal Inflammation in Mice. Am J Pathol. 2013;182(5):1617–28.
23. Yang S-S, Lo Y-F, Wu C-C, Lin S-W, Yeh C-J, Chu P, Sytwu H-K, Uchida S, Sasaki S, Lin S-H. SPAK-Knockout Mice Manifest Gitelman Syndrome and Impaired Vasoconstriction. J Am Soc Nephrol. 2010;21(11):1868.
24. Lan CC, Peng CK, Tang SE, Lin HJ, Yang SS, Wu CP, Huang KL. Inhibition of Na-K-Cl cotransporter isoform 1 reduces lung injury induced by ischemia-reperfusion. J Thorac Cardiovasc Surg. 2017;153(1):206–15.
25. Giaever I, Keese CR: **Micromotion of mammalian cells measured electrically**. *Proceedings of the National Academy of Sciences* 1991, **88**(17):7896.
26. Tiruppathi C, Malik AB, Del Vecchio PJ, Keese CR, Giaever I: **Electrical method for detection of endothelial cell shape change in real time: assessment of endothelial barrier function**. *Proceedings of the National Academy of Sciences* 1992, **89**(17):7919.
27. Szulcek R, Bogaard HJ, van Nieuw Amerongen GP. **Electric cell-substrate impedance sensing for the quantification of endothelial proliferation, barrier function, and motility**. *J Vis Exp* 2014(85):51300.
28. Shen C-H, Lin J-Y, Chang Y-L, Wu S-Y, Peng C-K, Wu C-P, Huang K-L: **Inhibition of NKCC1 Modulates Alveolar Fluid Clearance and Inflammation in Ischemia-Reperfusion Lung Injury via TRAF6-Mediated Pathways**. *Frontiers in Immunology* 2018, **9**(2049).

29. Johnston AM, Naselli G, Gonez LJ, Martin RM, Harrison LC, DeAizpurua HJ. SPAK, a STE20/SPS1-related kinase that activates the p38 pathway. Oncogene. 2000;19(37):4290–7.
30. Zhang J, Wang X, Vikash V, Ye Q, Wu D, Liu Y, Dong W. ROS and ROS-Mediated Cellular Signaling. Oxidative Med Cell Longev. 2016;2016:4350965–5.
31. Rao R. Oxidative stress-induced disruption of epithelial and endothelial tight junctions. Front Biosci. 2008;13:7210–26.
32. Overgaard CE, Daugherty BL, Mitchell LA, Koval M. Claudins: control of barrier function and regulation in response to oxidant stress. Antioxid Redox Signal. 2011;15(5):1179–93.
33. Diebold L, Chandel NS. Mitochondrial ROS regulation of proliferating cells. Free Radic Biol Med. 2016;100:86–93.
34. Hernanz R, Briones AM, Salaices M, Alonso MaJ. New roles for old pathways? A circuitous relationship between reactive oxygen species and cyclo-oxygenase in hypertension. Clinical science (London England: 1979). 2014;126(2):111–21.
35. Schlingmann B, Molina SA, Koval M. Claudins: Gatekeepers of lung epithelial function. Semin Cell Dev Biol. 2015;42:47–57.
36. Ohta H, Chiba S, Ebina M, Furuse M, Nukiwa T. Altered expression of tight junction molecules in alveolar septa in lung injury and fibrosis. American Journal of Physiology-Lung Cellular Molecular Physiology. 2011;302(2):L193–205.
37. Li G, Flodby P, Fau - Luo J, Luo J, Fau - Kage H, Kage H, Fau - Sipos A, Sipos A, Fau - Gao D, Gao D, Fau - Ji Y, Ji Y. Fau - Beard LL, Beard Ll Fau - Marconett CN, Marconett Cn Fau - DeMaio L, DeMaio L Fau - Kim YH et al: **Knockout mice reveal key roles for claudin 18 in alveolar barrier properties and fluid homeostasis**. (1535–4989 (Electronic)).
38. Chen W, Yazicioglu M, Cobb MH. Characterization of OSR1, a member of the mammalian Ste20p/germinal center kinase subfamily. J Biol Chem. 2004;279(12):11129–36.
39. Wang W, Weng J, Yu L, Huang Q, Jiang Y, Guo X. Role of TLR4-p38 MAPK-Hsp27 signal pathway in LPS-induced pulmonary epithelial hyperpermeability. BMC Pulm Med. 2018;18(1):178.

Figures

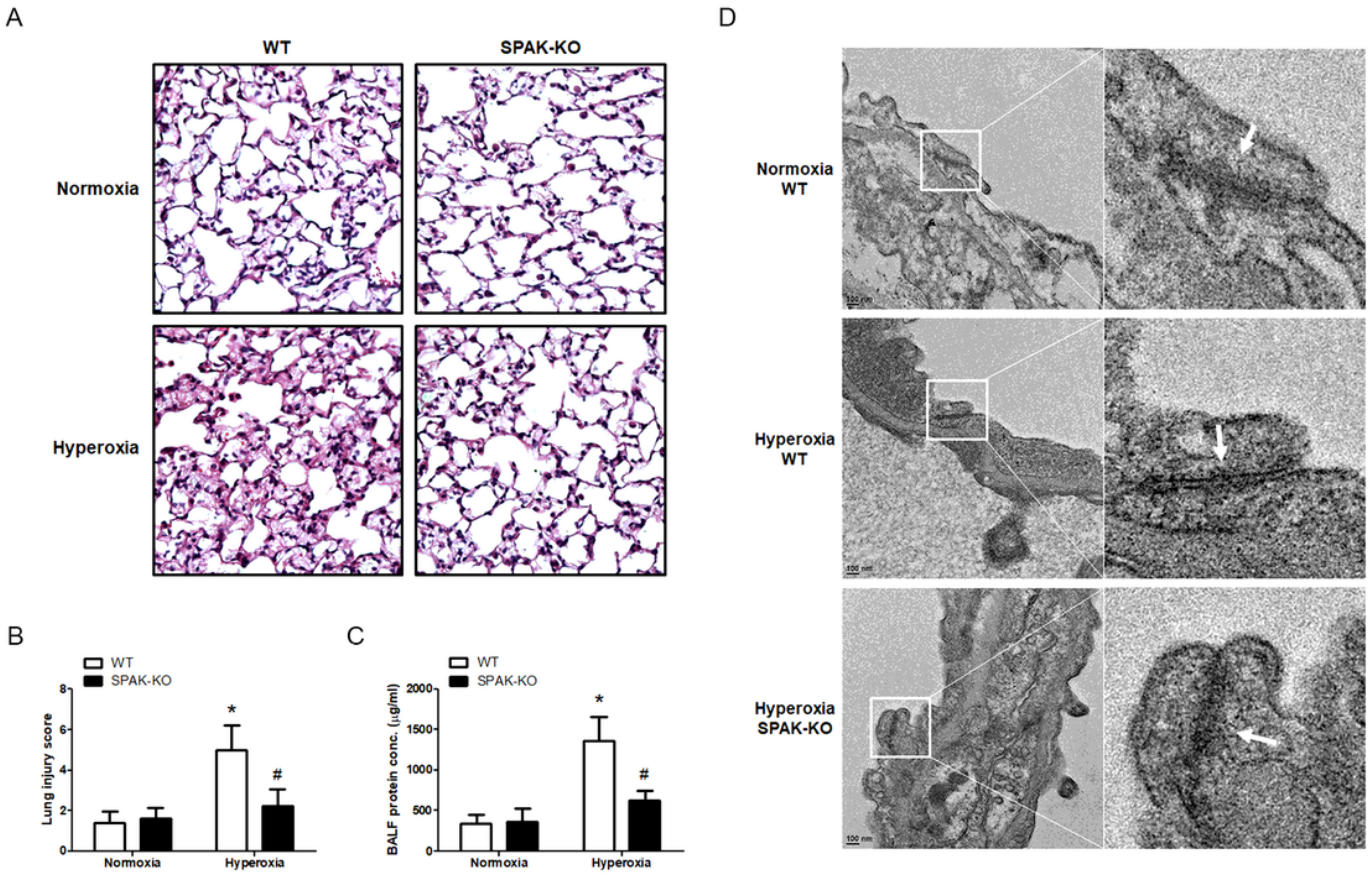

Figure 1

Effects of SPAK on the barrier integrity in hyperoxic acute lung injury. (A) Representative images of hematoxylin and eosin staining of mouse lungs (400 × magnification). (B) Lung injury score by histological evaluation of mouse lung tissues (n = 6). (C) Protein concentration in bronchoalveolar lavage fluid (n = 6). (D) Transmission electron microscopy for the morphology of tight junctions in alveolar epithelial cells (arrows). BALF: bronchoalveolar lavage fluid. WT: wild type. SPAK-KO: SPAK knock-out. Data are expressed as the means ± SD. *p < 0.05 versus normoxia WT; #p < 0.05 versus hyperoxia WT.

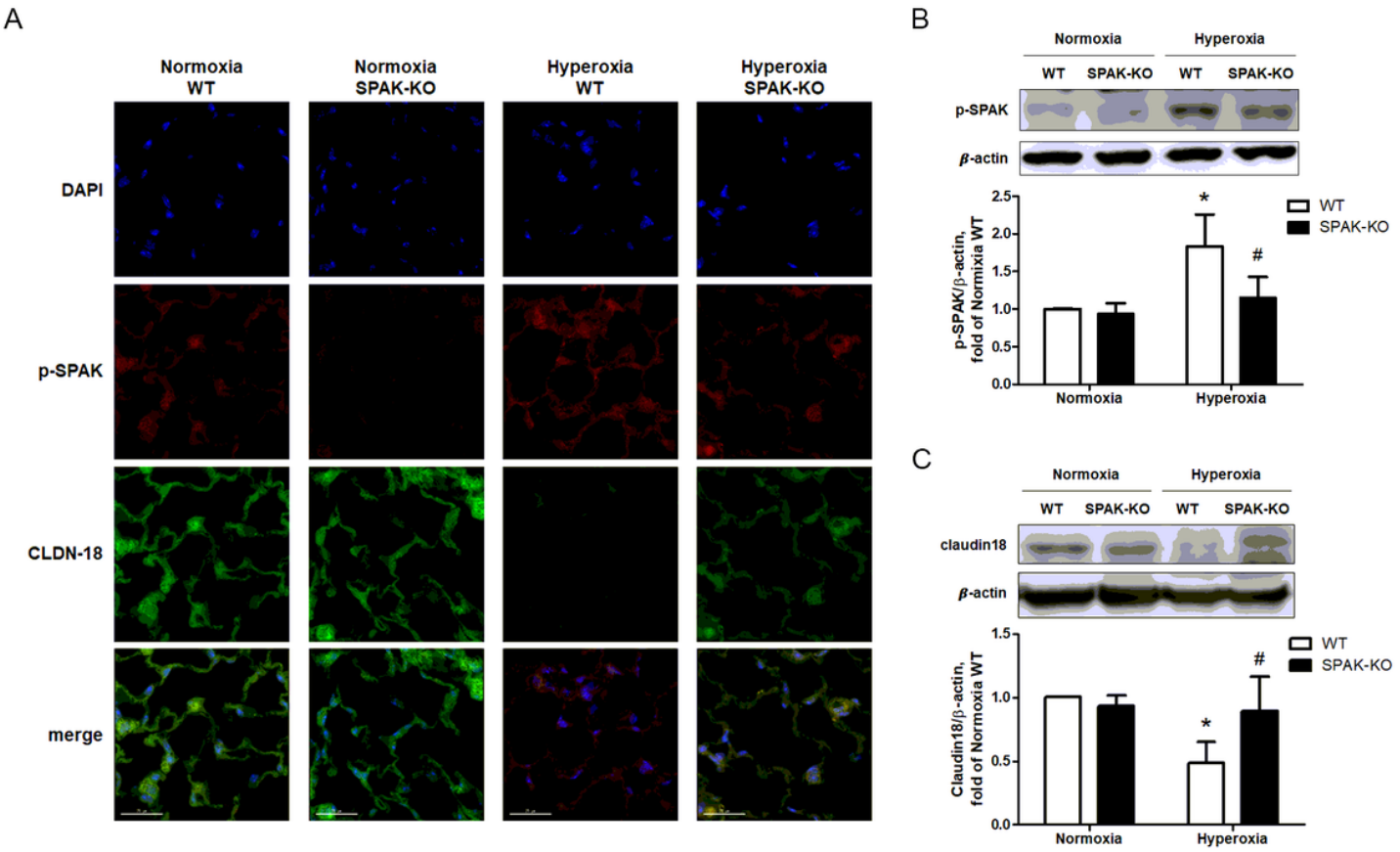

Figure 2

Effects of hyperoxia on the expressions of p-SPAK and claudin-18 of alveolar epithelium in hyperoxic acute lung injury. (A) Representative images of immunofluorescence staining for p-SPAK (TRITC-labeled red) and claudin-18 (FITC-labeled green) of mouse lungs (original magnification × 600). Nuclei were counterstained with DAPI (blue). (B) p-SPAK expressions in mouse lungs determined by western blot analysis (n = 5). (C) Claudin-18 expressions in mouse lungs determined by western blot analysis (n = 6). WT: wild type. SPAK-KO: SPAK knock-out. p-SPAK: phosphorylated-SPAK. Data are expressed as the means ± SD. *p < 0.05 versus normoxia WT; #p < 0.05 versus hyperoxia WT.

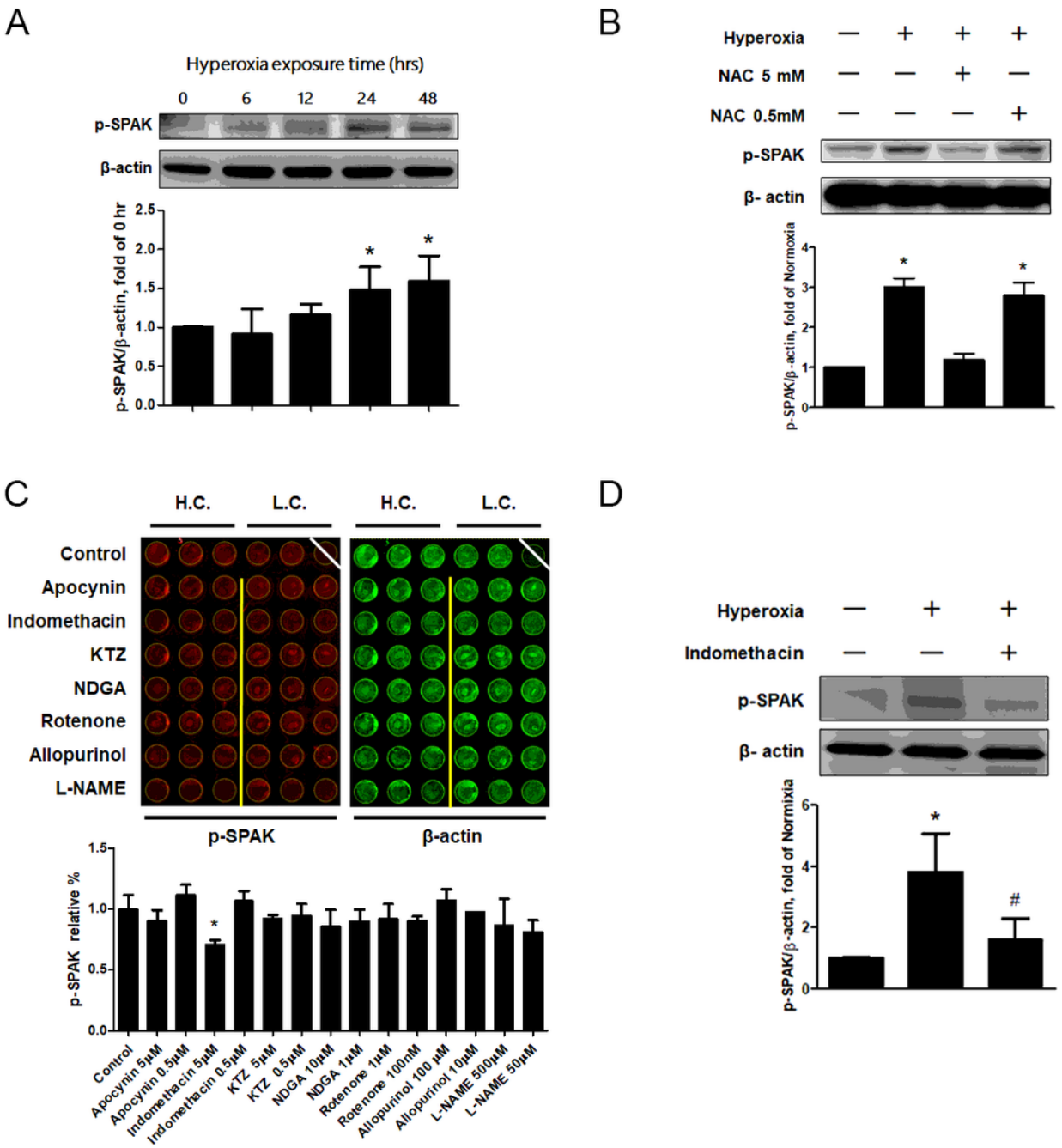

Figure 3

Effects of ROS on the expressions of p-SPAK in MLE-12 cells exposed to hyperoxia. (A) Effects of hyperoxia duration on p-SPAK expressions determined by western blot analysis (n = 4). * P < 0.05 versus 0 hour. (B) Effects of n-acetylcysteine pretreatment on p-SPAK expressions in MLE-12 cells exposed to hyperoxia determined by western blot analysis (n = 3). * P < 0.05 versus normoxia control; # P < 0.05 versus hyperoxia control. (C) Effects of ROS-generating enzyme inhibitors on p-SPAK expressions detected by in-cell western assay and the quantitative values from intensity of p-SPAK (n = 3). * P < 0.05 versus control. (D) Effects of indomethacin 5 μM on p-SPAK expressions determined by western blot analysis (n = 3). * P < 0.05 versus normoxia control; # P < 0.05 versus hyperoxia control. WT: wild type.

NAC: n-acetylcysteine. H.C.: high concentration. L.C.: low concentration. p-SPAK: phosphorylated-SPAK. Data are expressed as the mean ± SD.

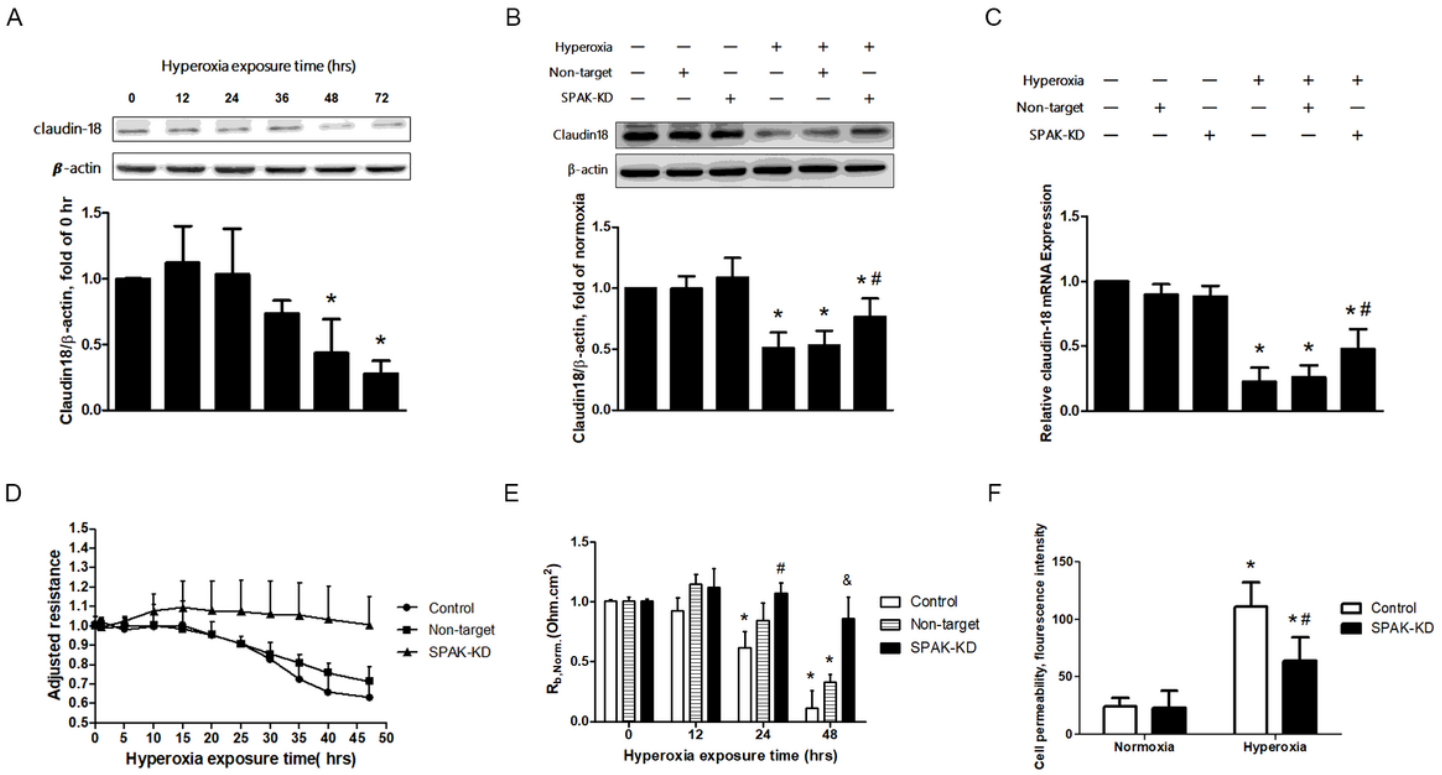

Figure 4

Effects of p-SPAK on the expressions of claudin-18 and barrier function in MLE-12 cells exposed to hyperoxia. (A) Effects of exposure duration on expressions of claudin-18 in MLE-12 cells determined by western blot analysis (n = 4). *p < 0.05 versus 0 hour. (B, C) Effects of SPAK-KD on expressions of claudin-18 in MLE-12 cells determined by western blot analysis and mRNA levels (n = 4). *p < 0.05 versus normoxia control; #p < 0.05 versus hyperoxia control. (D) Transepithelial electrical resistance of MLE-12 cells measured by ECIS (n = 4). (E) Barrier resistance (Rb) of MLE-12 cells measured by ECIS (n = 4). *p < 0.05 versus 0 hour control; #p < 0.05 versus 24 hour control; & P < 0.05 versus 48 hour control. (F) Paracellular permeability assay using MLE-12 cells cultured with FITC-dextran (n = 5). *p < 0.05 versus normoxia control; #p < 0.05 versus hyperoxia control. SPAK-KD: SPAK knock-down. Data are expressed as the means ± SD.

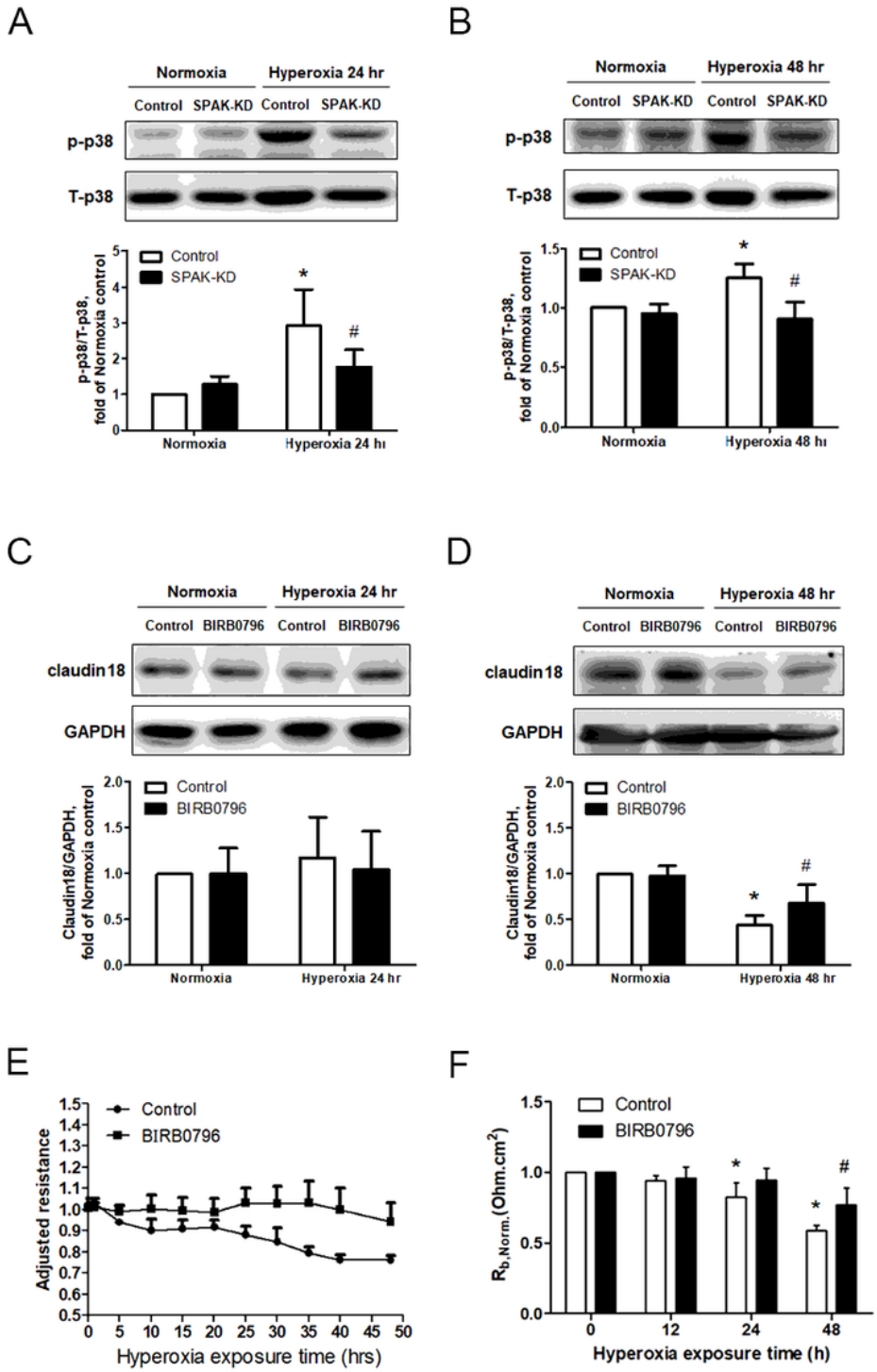

Figure 5

Effects of p38 MAPK on the expressions of claudin-18 and barrier function in MLE-12 cells after hyperoxic exposure. (A, B) Expressions of total p38 MAPK and phosphor brylated p38 MAP K after hyperoxic exposure for 24 hours (n = 6) and 48 hours (n = 6). *p < 0.05 versus normoxia control; #p < 0.05 versus hyperoxia control. (C, D) Claudin-18 expressions after treatment by p38 MAPK inhibitor BIRB-796 followed by exposure to hyperoxia for 24 hours (n = 6) and 48 hours (n = 5). *p < 0.05 versus normoxia

control; #p < 0.05 versus hyperoxia control. (E) Transepithelial electrical resistance treated by BIRB-796 and measured by ECIS (n = 4). (F) Barrier resistance (Rb) of MLE-12 cells measured by ECIS (n = 4). *p < 0.05 versus 0 hour control; #p < 0.05 versus 48 hour control. SPAK-KD: SPAK knock-down. T-p38: total-p38. p-p38: phosphorylated-p38. Data are expressed as the mean ± SD.

Supplementary Files

This is a list of supplementary files associated with this preprint. Click to download.

- AuthorChecklistARRIVE.pdf
- Originalwesternblotdata.pdf